Subnatural Linewidth Biphotons with Controllable Temporal Length

Shengwang Du,* Pavel Kolchin, Chinmay Belthangady, G. Y. Yin, and S. E. Harris
Edward L. Ginzton Laboratory, Stanford University, Stanford, California 94305, USA
(Received 31 December 2007; published 8 May 2008)

This Letter describes the generation of biphotons with a temporal length that can be varied over the range of 50–900 ns, with an estimated subnatural linewidth as small as 0.75 MHz. We make use of electromagnetically induced transparency and slow light in a two-dimensional magneto-optical trap with an optical depth as high as 62. We report a sharp leading edge spike that is a Sommerfeld-Brillouin precursor, as observed at the biphoton level.

DOI: 10.1103/PhysRevLett.100.183603 PACS numbers: 42.50.Gy, 37.10.Gh, 42.50.Dv, 42.65.Lm

Following the early papers of the Lukin and Kimble groups [1,2], it became apparent that it should be possible to use double-Λ systems for the generation of biphoton wave packets with temporal lengths that are controllable by varying the optical group velocity. Early results obtained at Stanford using a spherical magneto-optical trap (MOT) with an optical depth (OD) of about 10 [3,4] demonstrated wave packets with correlation times of about 50 ns and linewidths of about 9 MHz. In this Letter, we report the use of a two-dimensional (2D) MOT operating at an optical depth of 62 to attain major improvements in the performance of this type of biphoton source. These include generation of biphotons as long as 900 ns with linewidths as narrow as 0.75 MHz, a factor of 30 improvement in the effective dephasing rate of the nonallowed transition, a demonstrated efficiency of Stokes to anti-Stokes conversion of 74%, and operation in the regime where the temporal length of the biphoton varies inversely with the optical group velocity, thereby demonstrating that the physics suggested by Refs. [3,5] really works. This Letter also reports a sharp leading edge spike on the front edge of the generated biphoton. This spike is a Sommerfeld-Brillouin precursor [6] and is observed here by photon correlation.

We begin by motivating the need for a source of long and narrow-band biphotons: First, to efficiently absorb the biphotons and to store entanglement at distant locations, it is essential that the biphoton linewidth is less than the atomic linewidth [7]. Other applications benefit from the temporal length. For example, quantum teleportation requires that relative path lengths be stabilized to within the temporal length of the interacting photons, and long biphotons circumvent the need for stringent path length control [8].

There are other techniques that are now successfully used to lengthen generated biphotons. By using spontaneous parametric down-conversion (SPDC) in nonlinear crystals and cavities, paired photons with a linewidth of about 10 MHz and correlation times of about 50 ns are obtained [9]. An alternative approach has been demonstrated by Vuletic and colleagues, who generate degenerate biphotons with a temporal length of 100 ns [10]. Du *et al.*, by using four-wave mixing in a two-level system, have also demonstrated similar correlation times [11].

A schematic for biphoton generation is shown in Fig. 1. In the presence of counterpropagating, circularly polarized, cw pump (ω_p) and coupling (ω_c) lasers, phase-matched, paired Stokes (ω_s) and anti-Stokes ($\omega_{\rm as}$) photons are spontaneously generated and propagate in opposite directions. The essentials of the biphoton generation process are described by the coupled equations [3] for the frequency domain operators $a_s^\dagger(-\omega)$ and $a_{\rm as}(\omega)$:

$$\begin{aligned} \frac{\partial a_s^\dagger}{\partial z} + g_R a_s^\dagger + \kappa_s a_{\rm as} &= F_s \\ -\frac{\partial a_{\rm as}}{\partial z} + \Gamma a_{\rm as} + \kappa_{\rm as} a_s^\dagger &= F_{\rm as}. \end{aligned} \tag{1}$$

$\Gamma(\omega)$ describes the loss and dispersion of the electromagnetically induced transparency (EIT) profile, $g_R(\omega)$ is the (complex) Raman gain, $\kappa_s(\omega)$ and $\kappa_{\rm as}(\omega)$ are parametric coupling constants, and F_s and $F_{\rm as}$ are the Langevin operators. Expressions for each of these quantities are given in Refs. [3,5]. We make the assumption that the entire atomic population remains in the ground state; this assumption allows the different physical effects to be separated as in Eq. (1). More complete analyses have been given by Kolchin [5] and Ooi [12].

There are three characteristic times that determine the shape of the biphoton wave function [3,5]. The first is the

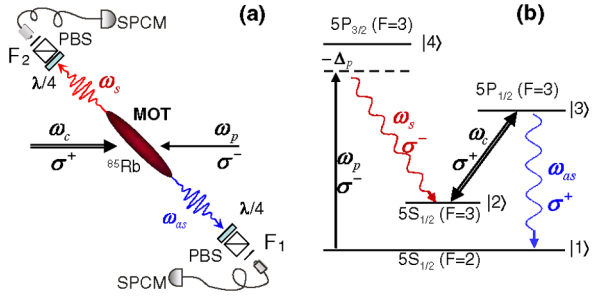

FIG. 1 (color online). Biphoton generation in a double-Λ system. (a) Experimental configuration. (b) ^{85}Rb energy level diagram. F_1 and F_2 are narrow-band optical frequency filters.

Rabi time $\tau_r = 2\pi/\Omega_c$, where Ω_c is the coupling Rabi frequency. The second is the relative group delay between the anti-Stokes and Stokes photons $\tau_g = L/V_g$, where L is the length of the medium and V_g is the anti-Stokes group velocity. This group delay time $\tau_g = (2\gamma_{13}/\Omega_c^2)N\sigma L$, where $N\sigma L$ is the optical depth and γ_{13} is the dephasing rate of level $|3\rangle$. The third characteristic time is the minimum pulse width required to pass through the EIT medium $\tau_{\min} = 8\ln(2)\gamma_{13}\sqrt{N\sigma L}/\Omega_c^2$ [13]. When $\tau_g < \tau_r$, the solution is oscillatory. When $\tau_g > \max[\tau_r, \tau_{\min}]$, we obtain the reasonably rectangular waveforms that are experimentally observed here. These near-rectangular waveforms may be understood from either the time or the frequency domain viewpoint [14]: In the time domain, the paired photons are always emitted from the same, but unknown, point in the medium. Therefore, the correlation function is rectangular with a temporal width of τ_g. In the frequency domain, one obtains the same result by noting that the phase mismatch factor $x = \Delta kL/2$ in the argument of $\sin(x)/x$ is $\omega\tau_g/2$. This factor determines the linewidth of $0.88/\tau_g$. (For SPDC in nonlinear crystals, the rectangular-shaped biphoton wave packet has been well known, but due to its subpicosecond correlation time, has not been directly measured [15].)

The experimental configuration is shown in Fig. 1(a). We use a 2D ^{85}Rb MOT with a cylindrical atomic cloud of length 1.7 cm and an aspect ratio of 25. As compared to the spherical trap that was used by Balić *et al.* [3], this configuration optimizes the optical depth and at the same time eliminates the longitudinal magnetic field gradient, thereby greatly reducing the inhomogeneous Zeeman broadening of the m states of the $5S_{1/2}$ level. With a transverse magnetic field gradient of about 10 Gauss/cm, we measure a dephasing rate of $\gamma_{12} = 0.02\gamma_{13}$. Of importance, the MOT magnetic field remains on throughout the experiment.

The trapping laser has a power of 160 mW and a beam diameter of 2 cm and is red detuned by 20 MHz from the $|5S_{1/2}, F = 3\rangle \rightarrow |5P_{3/2}, F = 4\rangle$ transition. A repumping laser is locked to the $|5S_{1/2}, F = 2\rangle \rightarrow |5P_{3/2}, F = 2\rangle$ transition and has a power of 80 mW. The experiment is run periodically with a MOT trapping time of 4.5 ms and a paired photon generation window of 0.5 ms. Towards the end of the trapping cycle and before the pump and coupling lasers are turned on, the atomic population is pumped to the ground level $|1\rangle = |5S_{1/2}, F = 2\rangle$ by turning off the repumping laser 0.3 ms before turning off the trapping laser. The pump laser at 780 nm is circularly polarized (σ^-), has a $1/e^2$ diameter of 1.46 mm, and is blue detuned from the $|1\rangle \rightarrow |4\rangle$ transition by 146 MHz, i.e., $\Delta_p = 48.67\gamma_{13}$. The coupling laser at 795 nm is circularly polarized (σ^+), has a $1/e^2$ beam diameter of 1.63 mm, and is on resonance with the $|2\rangle \rightarrow |3\rangle$ transition. The counterpropagating pump and coupling beams are collinear and set at a 2° angle from the longitudinal axis of the MOT. The Stokes (σ^-) and anti-Stokes (σ^+) photons are coupled into opposing single mode fibers after passage through $\lambda/4$ wave plates and polarization beam splitters (PBSs). The Stokes and anti-Stokes fiber coupling efficiency is 70%, and the $1/e^2$ waist diameter of their foci is 220 μm.

As shown in Fig. 1(a), further filtering includes 780 and 795 nm interference filters and Fabry-Perot etalons with bandwidths of 500 MHz in both the Stokes and anti-Stokes channels (F_1 and F_2). The transmission efficiency of the filters and etalons together is 45% in the Stokes channel and 40% in the anti-Stokes channel. Each single photon-counting module (SPCM) has a quantum efficiency of about 50%.

An objective of this work is to verify the relation between the optical group delay and the length of the biphoton waveform. The group delay is controlled by varying the optical depth and the coupling laser power. The optical depth could be varied over a range of about 5 up to 62. The measured group delay agreed well with the calculated value and could be varied from 50 to 900 ns.

Figure 2 shows the experimental and theoretical results at an optical depth of 7. Here the pump and coupling Rabi frequencies are $\Omega_p = 1.16\gamma_{13}$ and $\Omega_c = 4.20\gamma_{13}$, respectively. Optical transmission as a function of the anti-Stokes frequency is shown in Fig. 2(a). The (red) circles show the

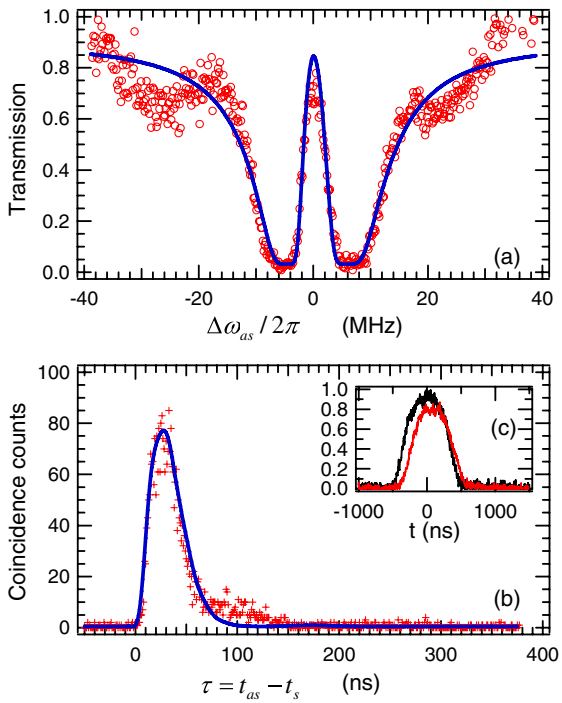

FIG. 2 (color online). Biphoton generation at OD = 7, $\Omega_c = 4.20\gamma_{13}$, $\Omega_p = 1.16\gamma_{13}$, and $\Delta_p = 48.67\gamma_{13}$. (a) Anti-Stokes EIT transmission profile. (b) Stokes–anti-Stokes coincidence counts per 1 ns bin in 800 s as a function of delay. (c) Propagation delay of the anti-Stokes pulse: The reference curve (black) centered at $t = 0$ is measured with the MOT turned off, and the delayed pulse (red) is measured with the MOT on.

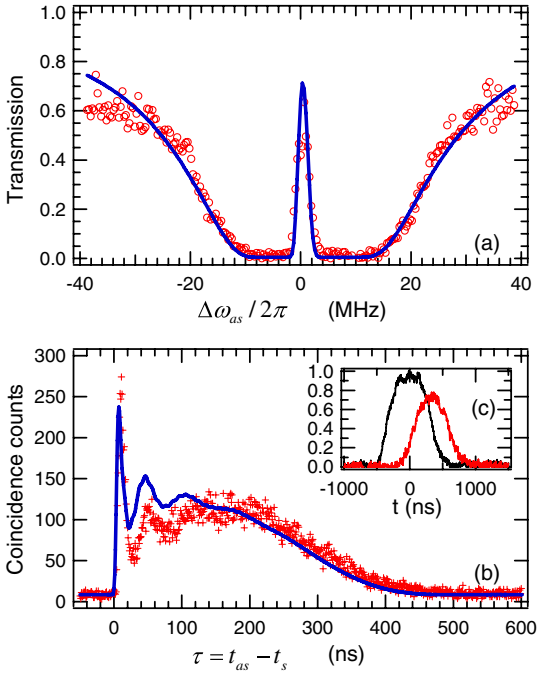

FIG. 3 (color online). Biphoton generation at OD = 53, $\Omega_c = 4.20\gamma_{13}$, $\Omega_p = 1.16\gamma_{13}$, and $\Delta_p = 48.67\gamma_{13}$.

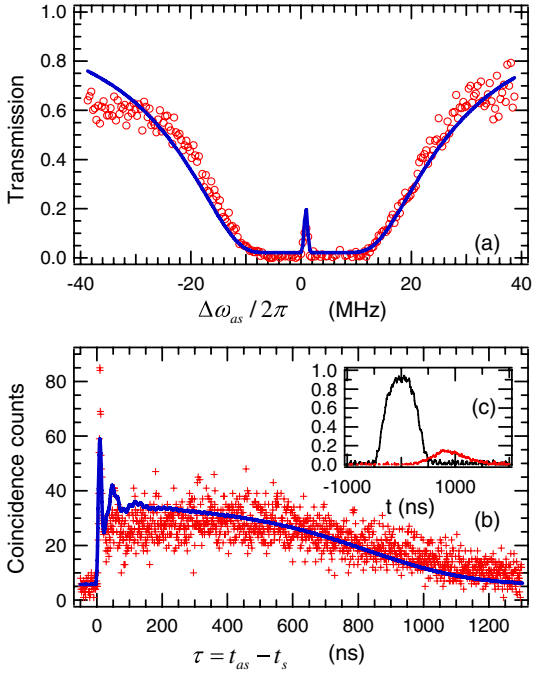

FIG. 4 (color online). Biphoton generation at OD = 53, $\Omega_c = 2.35\gamma_{13}$, $\Omega_p = 1.16\gamma_{13}$, and $\Delta_p = 48.67\gamma_{13}$.

experimental data, and the solid (blue) curve is the theoretical curve best fit for a dephasing rate $\gamma_{12} = 0.02\gamma_{13}$, OD = 7, and a vertical scaling factor. The measured Stokes–anti-Stokes coincidence counts (red +) are shown in Fig. 2(b), with a $1/e$ correlation time of 53 ns. The theoretical curve (solid, blue) is computed from $\eta T \Delta t G^{(2)}(\tau)$, where $G^{(2)}(\tau) = \langle a_s^\dagger(t) a_{\rm as}^\dagger(t+\tau) a_{\rm as}(t+\tau) a_s(t)\rangle$ is the Glauber correlation function, Δt is the time bin width, T is the total experimental time, and η is a vertical scale factor. The inset Fig. 2(c) shows a slow light measurement of an optical pulse at the anti-Stokes frequency with a group delay about $\tau_g = 50$ ns. In this case, $\tau_g \simeq \tau_r \simeq \tau_{\rm min} = 44$ ns, and the correlation function does not have a rectangular shape.

As we increase the optical depth and attain the regime where $\tau_g > \tau_{\rm min} > \tau_r$, we obtain a more rectangular biphoton waveform. Figure 3 shows the experimental results at OD = 53 with other parameters the same as in Fig. 2. The $1/e$ correlation time of 303 ns in Fig. 3(b) is very close to the group delay $\tau_g = 321$ ns given by the slow light measurement in Fig. 3(c). The two other characteristic times are $\tau_r = 79$ ns and $\tau_{\rm min} = 121$ ns. Figure 4 shows EIT, group delay, and the correlation obtained by reducing Ω_c to $2.35\gamma_{13}$ while maintaining the other parameters as in Fig. 3. At the expense of reduced transmission, the pulse delay and biphoton length are increased to about 900 ns.

Figure 5(a) plots measured correlation time as a function of measured group delay. The solid line is a linear least squares fit. We mention that the plots in Fig. 4 of Balić *et al.* [3] are in a damped Rabi oscillation regime and not in the linear group delay regime where $\tau_g > \tau_r$.

The linewidth of the generated biphotons is obtained by using the solution of Eq. (1) to fit the measured correlation profiles and then using this same solution to plot the biphoton emission profile in the frequency domain. The theoretical curves of Figs. 2(b), 3(b), and 4(b) are computed with all parameters obtained from the EIT measurements and vertically scaled to fit the experimental data. The calculated biphoton linewidths are 9.66, 2.36, and 0.75 MHz, respectively. These linewidths are comparable to the measured EIT bandwidths and in the latter two cases are less than the 6 MHz natural linewidth of Rb. This linewidth narrowing is consistent with the phase-matching bandwidth $(0.88/\tau_g)$. An alternate approach to estimate the linewidth is to assume transform-limited biphotons and to take the Fourier transform of $\sqrt{g^{(2)}(\tau) - 1}$, where $g^{(2)}(\tau)$ is

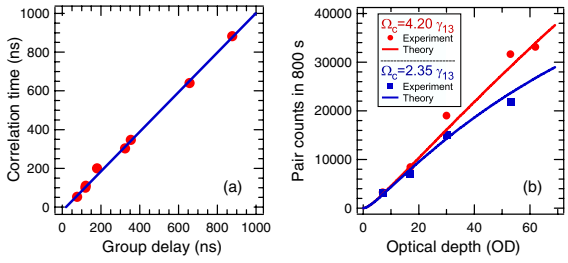

FIG. 5 (color online). (a) Measured correlation time vs measured anti-Stokes group delay. (b) Paired counts in a 1 ns bin in 800 s as a function of the optical depth.

the normalized correlation function [10]. By doing so, we obtain linewidths of 7.23, 1.95, and 0.71 MHz, respectively.

We turn next to the sharp peak at the leading edge of the correlation function of Figs. 3 and 4. Following Dan Gauthier's suggestion, this peak is the result of simultaneously generated Stokes and anti-Stokes photons that travel at nearly the speed of light in vacuum and arrive near-simultaneously at the photodetectors. In agreement with previous work on Sommerfeld-Brillouin precursors, we find that the duration of this peak corresponds to the inverse of the total opacity bandwidth and therefore varies approximately inversely with the square root of the optical depth. Though precursors are now understood in the optical region [16] and have even been observed long ago with correlated gamma-ray photons [17], this work reports the first observation of precursors as measured by single photon correlation.

To obtain the generation rate of our biphoton source, we take into account the filter and etalon transmissions, the fiber to fiber coupling efficiency, the detector quantum efficiencies, and the duty cycle. For the conditions of Figs. 2–4, we obtain generation rates of 1275, 12 569, and 8730 pairs/s, respectively. Higher generation rates can be achieved by increasing the pump laser power. With $\Omega_p = 6.88\gamma_{13}$, the paired photon generation rates are 4.0×10^4 and 9.0×10^4 pairs/s at OD = 17 and 30, respectively. Figure 5(b) shows that the number of paired counts varies linearly with the optical depth. Though the generation rate per spectral bandwidth varies as the square of the optical depth, the bandwidth reduces linearly with depth, thereby leading to the linear dependence. Experimentally, under optimum conditions, we observe 74% of the Stokes photons to be paired. We also observe that all of the correlation data violate the Cauchy-Schwarz inequality $[g^{(2)}_{s,\mathrm{as}}(\tau)]^2/[g^{(2)}_{s,s}(0)g^{(2)}_{\mathrm{as,as}}(0)] \leq 1$. The largest violation is a factor of 11 600.

The 2D MOT as described in this work is likely to allow immediate improvements in single photon read-write techniques [18,19], in EIT-based quantum memory [7,20], and in nonlinear optics with cold atoms [21,22]. Each of these areas requires the same ingredients as demonstrated here: i.e., low dephasing rate, subnatural linewidth, and high optical depth. For example, the efficiency of a nonlinear process continues to improve as the photon linewidth is reduced below the natural linewidth and is ultimately limited by the dephasing rate of the nonallowed transition.

A promising application for long biphotons is their use for the conditional generation of temporally shaped single photons: Here one of the emitted photons would be used as a trigger to fire an electro-optic light modulator that would shape the phase or amplitude of the other photon.

The work was supported by the Defense Advanced Research Projects Agency, the U.S. Air Force Office of Scientific Research, and the U.S. Army Research Office.

*dus@stanford.edu

[1] C. H. van der Wal *et al.*, Science **301**, 196 (2003).
[2] A. Kuzmich *et al.*, Nature (London) **423**, 731 (2003).
[3] V. Balić *et al.*, Phys. Rev. Lett. **94**, 183601 (2005).
[4] P. Kolchin *et al.*, Phys. Rev. Lett. **97**, 113602 (2006).
[5] P. Kolchin, Phys. Rev. A **75**, 033814 (2007).
[6] L. Brillouin, *Wave Propagation and Group Velocity* (Academic Press, New York, 1960).
[7] L.-M. Duan *et al.*, Nature (London) **414**, 413 (2001); S. Lloyd *et al.*, Phys. Rev. Lett. **87**, 167903 (2001).
[8] H. de Riedmatten *et al.*, Phys. Rev. Lett. **92**, 047904 (2004).
[9] Z. Y. Ou *et al.*, Phys. Rev. Lett. **83**, 2556 (1999); H. Wang *et al.*, Phys. Rev. A **70**, 043804 (2004); C. E. Kuklewicz *et al.*, Phys. Rev. Lett. **97**, 223601 (2006); J. S. Neergaard-Nielsen *et al.*, Opt. Express **15**, 7940 (2007).
[10] J. K. Thompson *et al.*, Science **313**, 74 (2006).
[11] S. Du *et al.*, Phys. Rev. Lett. **98**, 053601 (2007).
[12] C. H. R. Ooi *et al.*, Phys. Rev. A **75**, 013820 (2007).
[13] S. E. Harris *et al.*, Phys. Rev. Lett. **82**, 4611 (1999).
[14] M. H. Rubin *et al.*, Phys. Rev. A **50**, 5122 (1994).
[15] A. V. Sergienko *et al.*, J. Opt. Soc. Am. B **12**, 859 (1995).
[16] H. Jeong *et al.*, Phys. Rev. Lett. **96**, 143901 (2006).
[17] F. J. Lynch *et al.*, Phys. Rev. **120**, 513 (1960).
[18] D. Matsukevich and A. Kuzmich, Science **306**, 663 (2004).
[19] J. Laurat *et al.*, Opt. Express **14**, 6912 (2006).
[20] A. V. Gorshkov *et al.*, Phys. Rev. Lett. **98**, 123601 (2007).
[21] M. Yan *et al.*, Phys. Rev. A **64**, 041801(R) (2001).
[22] D. A. Braje *et al.*, Phys. Rev. A **68**, 041801(R) (2003).